Proceedings of the Combustion Institute 40 (2024) 105429

Contents lists available at ScienceDirect

Proceedings of the Combustion Institute

journal homepage: www.elsevier.com/locate/proci

Thermal diffusion, exhaust gas recirculation and blending effects on lean premixed hydrogen flames

T.L. Howarth [a,b,*], M.S. Day [c], H. Pitsch [a], A.J. Aspden [b]

[a] Institute for Combustion Technology, RWTH Aachen University, Aachen, 52056, Germany
[b] School of Engineering, Newcastle University, Newcastle-Upon-Tyne, NE1 7RU, UK
[c] Computational Science Center, National Renewable Energy Laboratory, Golden, CO 80401–3305, USA

ARTICLE INFO

Keywords:
Hydrogen
Exhaust gas recirculation
Soret effect
Fuel blending
Thermodiffusive instability

ABSTRACT

Thermodiffusively-unstable lean premixed hydrogen flames are investigated using two-dimensional direct numerical simulation employing finite-rate chemical kinetics. Three databases are generated focussing on the inclusion of the Soret effect, the recirculation of exhaust gas, and blending with methane. A simple rescaling of a classic thermal diffusion model is presented and shown to mimic multicomponent diffusion with very low computational cost and little-to-no loss in accuracy. It is also shown that a previously developed model for mean local flame speeds in lean premixed hydrogen flames [1] can still be used provided Soret effects are taken into account in one-dimensional calculations. The addition of exhaust gas to the unburned mixture is found to enhance thermodiffusive instability; the primary mechanism for this was shown to be the highly-efficient third-body nature of water, with the reduction of adiabatic flame temperature a second-order effect. Again, the existing mean local flame speed model proved sufficient. Finally, blending with methane was found to reduce the thermodiffusive response of the flame, more so than the existing model suggests, despite adjustment of the fuel Lewis number; an adapted model is presented to account for this.

1. Introduction

The study of thermodiffusively unstable lean premixed hydrogen flames has gained great interest recently due to the ongoing energy transition to carbon-free fuels. Lean conditions are employed to mitigate exhaust NO_x emissions associated with conditions close to stoichiometry. Under the lean condition, the high mobility of the fuel leads to diffusive focussing and enhanced reactivity in regions convexly curved towards to reactants. This phenomenon can be studied during the linear phase of flame development [2–4], or in the non-linear phase where the flame forms w-shaped structures referred to as 'flame fingers' [5,6] leading to enhanced mean local flame speeds which translate to faster-than-expected flames. Thermodiffusive effects still prove relevant in turbulent flames, where the turbulence and instability act synergistically to accelerate the flame further [7–10].

Recent attempts have been made to model either the global consumption-based flame speed in two-dimensional freely-propagating flames [11], or mean local flame speed in two-dimensional freely-propagating [1] and three-dimensional freely-propagating and turbulent flames [10]. Specifically, the model proposed in [1] relates the instability quantity ω_2 derived from linear stability analysis [12] to the mean local flame speed enhancement (stretch factor), with

$$\omega_2 = -(B_1 + \beta(\mathrm{Le}_{\mathrm{eff}} - 1)B_2 + \mathrm{Pr}B_3) \tag{1}$$

for constants B_i, Zel'dovich number β, effective Lewis number $\mathrm{Le}_{\mathrm{eff}}$ and Prandtl number Pr. The Zel'dovich number is given by

$$\beta = \frac{E_a(T_b - T_u)}{RT_b^2} \tag{2}$$

where the overall activation energy has been evaluated by varying the burning flux through displacement with argon [13]. The effective Lewis number (assuming lean mixtures) is given by

$$\mathrm{Le}_{\mathrm{eff}} = \frac{\mathrm{Le}_{\mathrm{O}} + A\mathrm{Le}_{\mathrm{F}}}{1 + A}, \quad A = 1 + \beta(\phi^{-1} + 1) \tag{3}$$

for oxidiser and fuel Lewis numbers Le_{O} and Le_{F}, and equivalence ratio ϕ. For two-dimensional freely-propagating flames, the local flame speed enhancement factor is given by

$$I_0 = \frac{s_F}{s_L} = \begin{cases} \exp(0.057\omega_2), & \text{if } p < \Pi_c \\ 1 + 0.22\omega_2, & \text{otherwise} \end{cases} \tag{4}$$

where s_F is the freely-propagating flame speed, s_L is the unstretched laminar flame speed and Π_c is the normalised pressure associated with

* Corresponding author at: Institute for Combustion Technology, RWTH Aachen University, Aachen, 52056, Germany.
E-mail address: t.howarth@itv.rwth-aachen.de (T.L. Howarth).

https://doi.org/10.1016/j.proci.2024.105429
Received 4 December 2023; Accepted 13 June 2024
Available online 24 June 2024

a local maximum of ω_2, which for pure hydrogen–air flames takes the form

$$\Pi_c = \left(\frac{20\phi}{7 - 2\Theta} \right)^{150/(21+10\Theta)} \tag{5}$$

for equivalence ratio ϕ and non-dimensional temperature $\Theta = T/T_{\text{ref}}$, $T_{\text{ref}} = 300\text{K}$; interested readers are referred to [1] for more details. It should be emphasised that previous studies relating to this modelling strategy [1,10] have only focused on pure hydrogen–air flames.

Diffusive transport of species due to temperatures gradients, referred to as simply thermal diffusion or the Soret effect, is typically neglected in multi-dimensional simulations, however, its effect on premixed hydrogen flames can be significant [14–17]. The thermal diffusion coefficients for molecular and atomic hydrogen are negative, which increases the diffusive flux of H_2 into, and H out of, the reaction zone. As such, the Soret effects will exacerbate the thermodiffusive effects in lean hydrogen flames.

Exhaust gas recirculation is a technique typically employed in engineering applications to reduce NO_x emissions as the increased volume of inert species from the exhaust gas (e.g. H_2O or CO_2) reduces the adiabatic flame temperature due to increased heat capacity of the mixture, reducing the amount of thermal NO_x that can be produced. The reduction of adiabatic flame temperature increases the value of Zel'dovich number, and so will have effects on the thermodiffusive response of the flame.

Blending hydrogen with another fuel allows for utilising the advantages of both hydrogen (carbon-free, high reactivity) and another fuel. For example, in the case of methane, blending with hydrogen provides a way to significantly reduce carbon emissions while keeping the flame speed to a moderate value and avoid the dangers of flashback. There have been several studies performed examining differential diffusion effects in CH_4/H_2 flames [18–20], and there is a general agreement that thermodiffusive effects become more prominent with increased hydrogen content, which decreases the Markstein number, potentially changing its sign to an unstable negative value.

The aim of this work is to determine the generality of the model developed in [1], and understand the interaction between thermodiffusive instability with other external factors. Specifically, there are three overall objectives. Firstly, Soret effects are modelled and studied to determine whether the existing model for mean local flame speed can capture the additional thermodiffusive response anticipated. Secondly, the effects of exhaust gas recirculation are studied to determine how it interacts with thermodiffusive instability, why the response changes from undiluted cases, and whether the model can replicate the effect; this is the first study to consider the effect of exhaust gas recirculation on the thermodiffusive response of hydrogen flames. Finally, cases of hydrogen blended with methane will be considered to assess whether the existing model can also predict the anticipated change in thermodiffusive response of the flame.

A brief description of the solver used and a list of conditions used in each DNS database is given in Section 2, followed by an outline of the thermal diffusion model employed and its effects in Section 3. In Section 4, the effects of exhaust gas recirculation are quantified and explained, and the effect of the addition of methane to the mixture is modelled in Section 5.

2. Simulation configuration

Three databases have been created consisting of direct numerical simulations of two-dimensional laminar freely-propagating flames using finite-rate chemistry using PeleLMeX [21]. PeleLMeX solves the low-Mach-number equation set for reacting flow, where the fluid is treated as a mixture of ideal gases. A mixture-averaged model is employed for the species diffusion coefficients, and the addition of a thermal diffusion model is discussed in Section 3. The discretisation couples a multi-implicit spectral deferred correction approach for the integration of mass, species and energy equations with a density-weighted approximate projection method, which has incorporated spatially constant thermodynamic pressure through a velocity divergence constraint. Further details can be found in [22,23]. The databases are summarised as follows, with all combinations of conditions in {} simulated:

- Database A (with/without Soret, 48 cases):
  - $\phi \in \{0.3, 0.4, 0.5\}$
  - $T_u \in \{300, 400\}$ K
  - $p \in \{1, 3.5, 10, 20\}$ atm
- Database B ($T_u = 400$ K, 30 cases):
  - $\phi \in \{0.3, 0.4, 0.5\}$
  - $p \in \{1, 6\}$ atm
  - $\chi_{\text{EGR}} \in \{0, 0.05, 0.1, 0.15, 0.2\}$
- Database C ($T_u = 300$ K, 64 cases):
  - $\phi \in \{0.35, 0.45, 0.55, 0.65\}$
  - $p \in \{1, 3.5, 10, 32\}$ atm
  - $\chi_{H_2} \in \{0.55, 0.7, 0.85, 1\}$

Several tables are provided as supplementary material listing all conditions with corresponding flame speed, thermal thickness and instability parameter ω_2. In all databases, domains were set as $80l_F \times 640l_F$ with a base grid resolution of 128×1024 and 3 levels of adaptive mesh refinement leading to an effective resolution of 1024×8096 in a buffer region of 3 fine grid cells around the locations where the mass fraction of HO_2 exceeded 30% of the maximum value found in the corresponding one-dimensional simulation. The value of l_F (the freely-propagating thermal thickness) was predicted using the model from [1]. One-dimensional profiles generated by Cantera [24] were imposed with a random sinusoidal perturbation and used to initialise the simulations; each simulation was allowed to evolve for a sufficiently long time to allow development of flame instabilities prior to extracting statistics for analysis.

3. Thermal diffusion

Thermal diffusion of species is typically only possible through the usage of multicomponent transport models which are notoriously computationally expensive, particularly in multi-dimensional simulations. In this section, the mixture-averaged model developed by Chapman and Cowling [25], which is known to overestimate Soret effects [26], is rescaled to reflect multicomponent thermal diffusion. An assessment is then performed examining the effects of thermal diffusion on existing models for the mean local flame speed enhancement in lean premixed hydrogen flames.

3.1. Thermal diffusion model

For a species k, the mixture-averaged thermal diffusion velocity is given by

$$\mathbf{S}_k = -\frac{D_{k,mix}\Theta_k}{X_k}\frac{1}{T}\nabla T \tag{6}$$

where $D_{k,mix}, \Theta_k$ and X_k are the mixture-averaged diffusion coefficient, thermal diffusion ratio and mole fraction of species k respectively, and T is the temperature. Pele evaluates $D_{k,mix}$ by preprocessing the chemical mechanism to obtain $\log(D_{k,mix})$ in terms of a third-order polynomial in $\log(T)$. A similar approach can be taken to model Θ_k, where the model of the Chapman and Cowling is taken and fitted to a polynomial of T (rather than $\log(T)$). Thermal diffusion for species with molecular

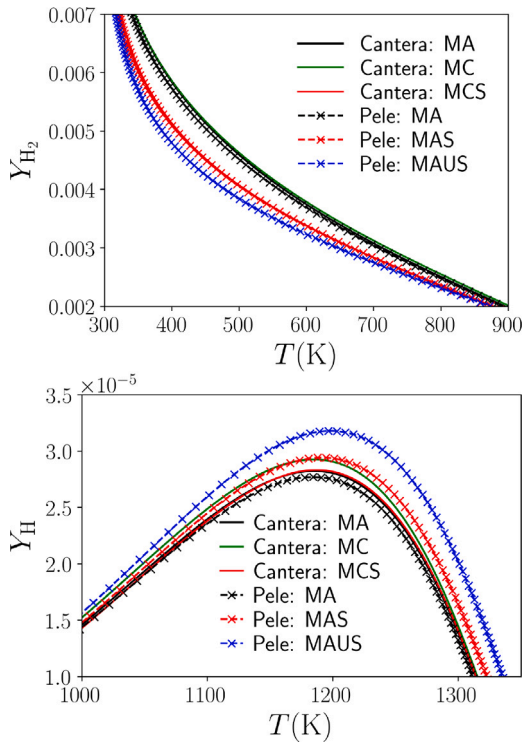

Fig. 1. Profiles of molecular (top) and atomic (bottom) hydrogen as functions of temperature, comparing the usage of different transport models (mixture-averaged, multicomponent, multicomponent with Soret, mixture-averaged with Soret and mixture-averaged with unadjusted Soret) between the two solvers (Cantera and Pele). Each line corresponds to individual flames performed with the respective transport models and solver. (For interpretation of the references to colour in this figure legend, the reader is referred to the web version of this article.)

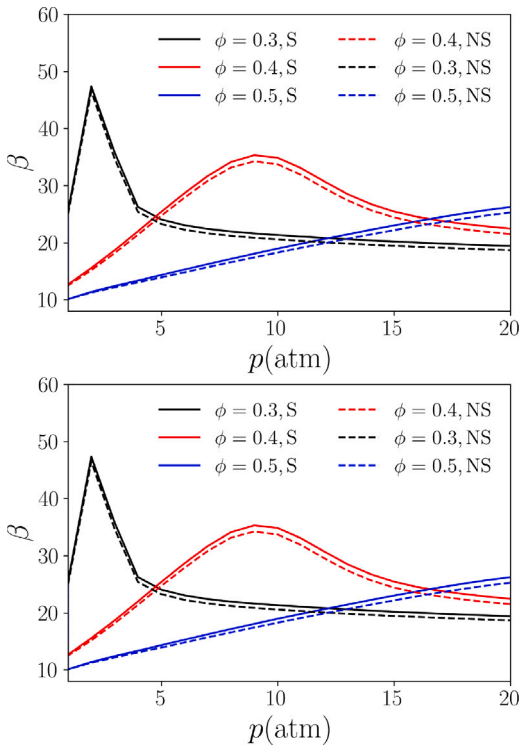

Fig. 2. Zel'dovich number as a function of pressure for $T_u = 300$ K (top) and $T_u = 400$ K (bottom), with different lines corresponding to the three equivalence ratios $\phi = 0.3, 0.4, 0.5$. Simulations with(S)/without(NS) the Soret effect employed are shown with solid/dashed lines respectively. (For interpretation of the references to colour in this figure legend, the reader is referred to the web version of this article.)

weights $W_k \geq 5$ is neglected. Specifically, the mixture-averaged thermal diffusion ratio Θ_k is given by

$$\Theta_{k,\mathrm{MA}} = \sum_{j \neq k}^{N} \theta_{kj} \tag{7}$$

where the binary coefficient θ_{kj} is given by

$$\theta_{kj} = f(T) X_k X_j \tag{8}$$

and the function $f(T)$ is a third-order polynomial fit in temperature to a function involving ratios of collision integrals and molecular weights (see [27] for more details). Following an approach similar to [28], the thermal diffusion ratios computed here are scaled to match multicomponent thermal diffusion ratios (to prevent an overestimation in magnitude) calculated from 1D simulations in Cantera i.e.

$$\Theta_{k,\mathrm{MC}} = \alpha_k \Theta_{k,\mathrm{MA}} \tag{9}$$

with the MC subscript denoting the coefficient derived from a multicomponent formulation, and MA subscript denoting the mixture-averaged value. Three different mechanisms were employed [29–31] to determine the appropriate values for α_k, considering all combinations of $\phi \in \{0.4, 0.7, 1\}, T_u \in \{300, 500, 700\}$ K, $p \in \{1, 5, 10, 20\}$ atm, resulting in 108 different simulations. A linear best fit suggests that $\alpha_{H_2} = 0.664$ and $\alpha_H = 0.580$ across all mechanisms, indicating that the scaling is insensitive to the choice of mechanism; a figure is provided as supplementary material showing this near-perfect correlation.

In this work, the thermal diffusion ratios used are given by $\Theta_k = \alpha_k \Theta_{k,\mathrm{MA}}$ for $k = \mathrm{H}, \mathrm{H_2}$. To validate this model, Fig. 1 compares species profiles with respect to temperature for the different transport models for 1D simulation at $\phi = 0.37, T_u = 300$ K, $p = 1$ atm, using the mechanism from [30]. The different transport models are denoted as follows: mixture-averaged (MA), multicomponent (MC), multicomponent with Soret (MCS), mixture-averaged with Soret (MAS, includes α_k adjustment), mixture-averaged with unadjusted Soret (MAUS). MA, MC and MCS profiles are available from Cantera, whereas MA, MAS and MAUS profiles are computed in Pele. The target profile is the MCS profile from Cantera. In the case of molecular hydrogen, the MA profiles (black solid and crosses) from Cantera and Pele line up very well with the MC profile from Cantera (solid green), indicating little-to-no benefit of using multicomponent diffusion (without the presence of thermal diffusion) over a standard mixture-averaged formulation (MA). However, a distinct shift is noted with the addition of thermal diffusion (MC, solid green to MCS, solid red line), with the increased drop in mass fraction of hydrogen resulting from the additional species diffusion induced across the temperature gradient. Without the scaling of the thermal diffusion coefficient, this increased diffusivity is overestimated (MAUS, blue crosses), with the tempering of the coefficient bringing the red crosses (MAS) back in line with the solid red line (MCS) as desired. In the case of atomic hydrogen, most profiles are very close to each other, other than the MAUS simulation where a noticeable overestimation in the mass fraction is observed. A figure is provided as supplementary material demonstrating the overestimation in magnitude, and correction through α_k, of the thermal diffusion coefficients in the MAUS and MAS profiles compared to the MCS profile.

3.2. Effects of thermal diffusion

The additional diffusivity of hydrogen is anticipated to enhance thermodiffusive instability of the flame. In fact, in all 1D simulations considered, the inclusion of Soret effects increases the Zel'dovich number (see Fig. 2), which in turn increases the value of ω_2.

To assess whether the increase in ω_2 translates into the multi-dimensional setting, Database A is analysed, with 24 different conditions considered, each with and without the mixture-averaged thermal

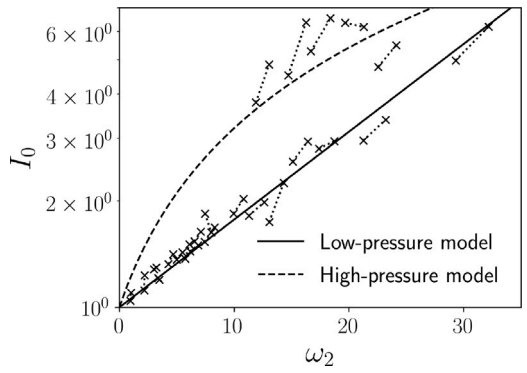

Fig. 3. Normalised freely-propagating flame speed (stretch factor) as a function of the instability parameter ω_2. Points are paired based on the same condition with and without Soret effects included, and the lines are given by Eq. (4). Note that the value of s_L used here in cases considering the Soret effects is different from those without it.

diffusion model discussed above included. The metric used to assess the response is the scaling of the mean local flame speed s_F, calculated as

$$s_F = -\frac{1}{(\rho Y_{\mathrm{H_2}})_u A_\Gamma} \int_\Omega \rho \dot{\omega}_{\mathrm{H_2}} \mathrm{d}\Omega \tag{10}$$

where subscript u denotes unburned value, Ω is the simulated domain and A_Γ is the area of the instantaneous isosurface obtained for $c_F = 0.9$, c_F the fuel-based progress variable

$$c_F = 1 - \frac{Y_{\mathrm{H_2}}}{Y_{\mathrm{H_2},u}} \tag{11}$$

where $Y_{\mathrm{H_2}}$ is mass fraction of hydrogen, and u denotes the unburned value [1,6]. s_F is then normalised by unstretched laminar flame speed s_L to give the mean local flame speed enhancement, also known as the stretch factor I_0 (see Eq. (4)). Mean local flame speed enhancement is plotted against the instability parameter ω_2 (see Eq. (1)) in Fig. 3. Each pair of data points correspond to matching conditions with and without thermal diffusion; in each case, thermal diffusion results in a higher value of ω_2. Generally, higher mean local flame speeds are seen with the inclusion of thermal diffusion; cases that decrease only do so slightly, and within the standard deviation of the value of s_F of the averaging period. In fact, good agreement is still seen with the previously developed model (Eq. (4)), provided that Soret effects are included in the corresponding 1D calculation.

4. Effect of exhaust gas recirculation

In this section, the effects of exhaust gas recirculation (EGR) are analysed; the parameter that describes the amount of exhaust gas present is the EGR fraction

$$\chi_{\mathrm{EGR}} = \frac{X_{\mathrm{EGR}}}{X_{\mathrm{R}} + X_{\mathrm{EGR}}}, \tag{12}$$

where X_{R} and X_{EGR} are the mole fractions of the reactants and recirculated products respectively. The recirculated products are computed based on the equilibrium mole fractions of the reactant condition, and consists of both air and steam.

By adding exhaust gases to the unburned mixture, a large amount of the heat energy released by the flame is used to heat up additional inert gases in the mixture, and this decreases the adiabatic flame temperature (see top of Fig. 4). As such, by construction of the Zel'dovich number, more instability would be expected with increasing χ_{EGR}. Furthermore, the overall activation energy increases with increasing blend fraction (see middle Fig. 4); in fact, this effect dominates the profile for the Zel'dovich number at the bottom of Fig. 4.

With increasing pressure, increasing overall activation energy results from the increased importance of the termolecular reaction H + O_2 + M $\rightleftharpoons$ HO_2 + M [1,32]. With EGR, H_2O acts as a highly-efficient third-body and so a similar effect is seen. To demonstrate the importance of the high third-body efficiency of H_2O, the same 1D simulations have been run to obtain the overall activation with the third-body coefficient reduced to same as N_2 (which is equal to 1). The variation in overall activation energy is now considerably different (Fig. 5); importantly, for cases $\phi \geq 0.4$ it has been significantly reduced. For the lean, high-pressure case ($\phi = 0.3, p = 6$ atm), the trend reverses due to a transition to the high-pressure regime, where weak chain-branching reactions are activated, releasing H and OH radicals and reducing the overall activation energy [32].

Specifically, for the case $\phi = 0.4, T_u = 400$ K, $p = 6$ atm, $\chi_{\mathrm{EGR}} = 0.15$, this leads to ω_2 reducing from 23.8 to 10.6. This small change in the chemical mechanism on the thermodiffusive response of the flame is shown in Fig. 6, where the aforementioned condition has been simulated with the reduced third-body efficiency coefficient. The flame has larger cellular structures (even though both domains are $80 l_F$ wide), smaller overshoots in postflame temperatures (the pink regions), and the stretch factor has decreased from 5 to 1.75, indicating significantly less of a thermodiffusive response.

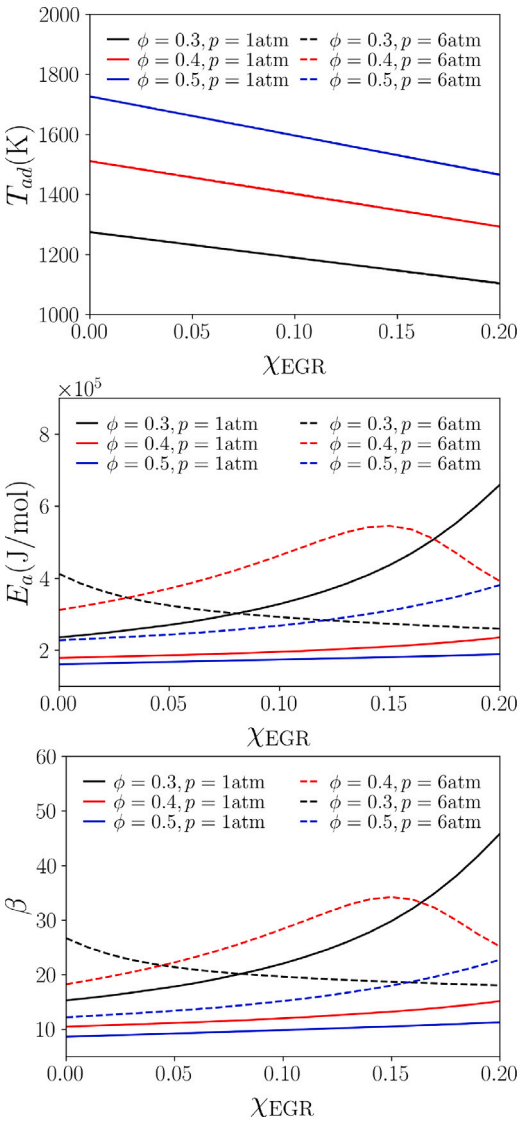

Fig. 4. Adiabatic flame temperature (top), overall activation energy (middle) and Zel'dovich number (bottom) with increasing volume of EGR for cases in Database B. (For interpretation of the references to colour in this figure legend, the reader is referred to the web version of this article.)

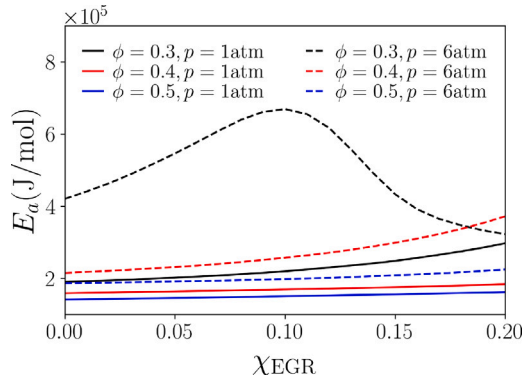

Fig. 5. Overall activation energy with increasing volume of EGR after reducing the third-body efficiency of H_2O in the reaction $H + O_2 + M \rightleftharpoons HO_2 + M$; compare this to the middle panel in Fig. 4. (For interpretation of the references to colour in this figure legend, the reader is referred to the web version of this article.)

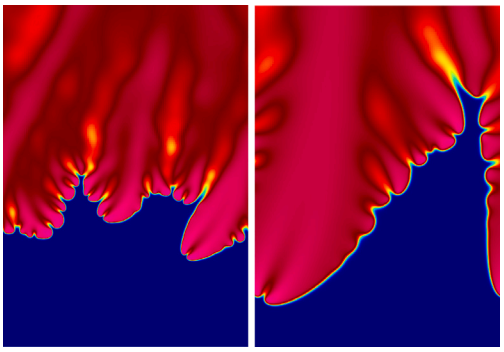

Fig. 6. Image of temperature field before (left) and after (right) reducing the third-body efficiency of H_2O.

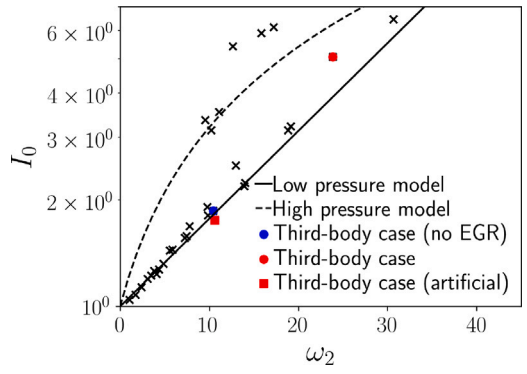

Fig. 7. Normalised freely-propagating flame speed as a function of the instability parameter ω_2. Every case is shown with a black cross, with points of comparison for cases with third-body coefficient manipulation shown in colour. (For interpretation of the references to colour in this figure legend, the reader is referred to the web version of this article.)

In terms of the existing model (Eq. (4)), good agreement is still found and can be seen in Fig. 7 by examining all cases from Database B. The case with the artificial third-body coefficient is explicitly shown with the realistic counterpart, along with the case from the same condition with $\chi_{EGR} = 0$. By comparing the artificial and non-EGR case, it is clear that without this third-body effect, the EGR has essentially no effect on the stretch factor.

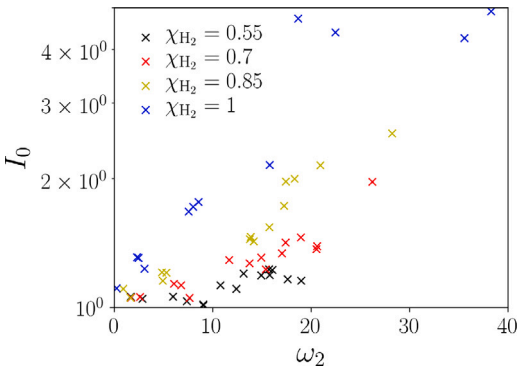

Fig. 8. Stretch factor as a function of the instability parameter ω_2. Colours are grouped into different values of χ_{H_2}. (For interpretation of the references to colour in this figure legend, the reader is referred to the web version of this article.)

5. Effect of blending

This section considers the thermodiffusive response of hydrogen-methane fuels blends; the parameter that describes the degree of blending is the blend fraction

$$\chi_{H_2} = \frac{X_{H_2}}{X_{H_2} + X_{CH_4}} \tag{13}$$

where X_{H_2} and X_{CH_4} are the mole fractions of hydrogen and methane respectively. For blends, there are three different ways to formulate a Lewis number, either diffusion-based, volume-based or heat-release-rate-based [33,34]. Here, we chose the diffusion-based formulation [19], given by

$$\frac{1}{Le_F} = \frac{\chi_{H_2}}{Le_{H_2}} + \frac{1 - \chi_{H_2}}{Le_{CH_4}}. \tag{14}$$

This weighted Lewis number value is in lieu of the fuel Lewis number Le_F in the expression for Le_{eff} (see Eq. (3)). To account for the methane in the fuel blend, the progress variable is now defined as

$$c_F = 1 - \frac{Y_{CH_4} + Y_{H_2}}{(Y_{CH_4} + Y_{H_2})_u} \tag{15}$$

which remains consistent with fuel-based progress variables at the pure hydrogen/methane-air limits; again, a progress variable value of $c_F = 0.9$ is used. Good alignment of this progress variable with the heat release is shown in supplementary material, along with a comparison to three other progress variable choices.

Fig. 8 shows the stretch factor of cases from Database C against ω_2 on a semilog scale with the original model (4). Although a positive correlation is observed, the collapse across different values of χ_{H_2} is unsatisfactory. However, it can also be seen that with decreasing value of χ_{H_2}, the constant of proportionality decreases. Therefore a new model is suggested of the form

$$I_0 = \frac{s_F}{s_L} = \exp(\alpha\omega_2 f(\chi_{H_2})) \tag{16}$$

under the constraint $f(0) = 0, f(1) = 1$. Plotting this function suggests a non-linear power law, so a function is taken of the form $f(\chi_{H_2}) = \chi_{H_2}^{\beta}$; by fixing $\alpha = 0.057$ to ensure consistency with the original model, a best-fit gave the value $\beta = 3.3$. Fig. 9 shows the calculated flame speed against the modelled value; note that some points in the pure hydrogen case were ignored here as they sit in the high-pressure regime ($p > \Pi_c$). For cases in this regime, it would be expected that an adjustment would be required to the high-pressure model (see Eq. (4)).

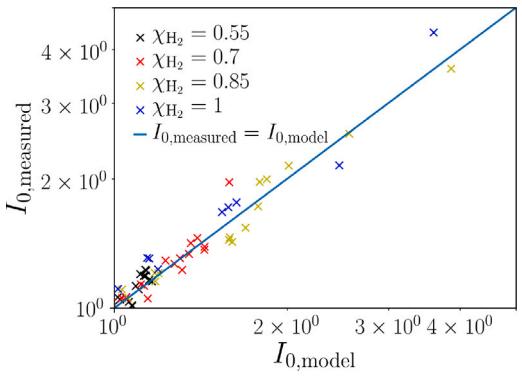

Fig. 9. Measure stretch factor against modelled stretch factor. Colours are grouped into different values of χ_{H_2}. (For interpretation of the references to colour in this figure legend, the reader is referred to the web version of this article.)

6. Discussion and conclusions

Three extensive databases of direct numerical simulations of two-dimensional lean premixed hydrogen flames have been analysed quantifying the effects of thermal diffusion, exhaust gas recirculation and blending hydrogen with methane.

Firstly, the mixture-averaged thermal diffusion model of Chapman and Cowling [25] was fit to polynomials in temperature and rescaled to replicate multicomponent diffusion (Fig. 1). This in turn was used to demonstrate that the existing model for mean local flame speed enhancement still provides good predictions; specifically, Eq. (4) closely models the ratio of freely-propagating flame speed s_F to the corresponding laminar value s_L (where the F and L values either both account for Soret, or both do not include Soret). There is nothing to suggest that previous work (e.g. [1,10]) is deficient because Soret effects were not included; i.e. while the flame speeds are generally higher, the flame physics/phenomenology is unaffected by inclusion of Soret effects.

Secondly, the addition of recirculated exhaust gas was found to increase the thermodiffusive response of the flame. The leading-order mechanism for this was the added H_2O acting as an efficient third-body in the reaction $H + O_2 + M \rightleftharpoons HO_2 + M$, which decreases the overall size of the radical pool and increases the overall activation energy (Figs. 5 and 6). The decrease in adiabatic flame temperature due to higher heat capacity from additional diluents was a secondary effect. This was further demonstrated through a simulation where the third-body coefficient H_2O was reduced to that of N_2 and the stretch factor reduced by a factor of 65%. This also demonstrates the sensitivity of thermodiffusive instability to parameters related to the kinetics, in addition to the transport properties. The existing model was shown to continue to capture the mean local enhancement well, including variations to the third-body coefficient (Fig. 7). The role of radiation was neglected in this particular study (the largest mass fraction of water in the reactants is 2.5%), however, some readsorption of heat in the reactants due to the presence of water is expected [35], and will be the focus of future work.

Finally, the blending of methane with hydrogen was found to decrease the level of instability as expected, however an additional parameter was required to be added to the model in the form of the blend fraction χ_{H_2} (Fig. 9), and is given by the equation

$$I_0 = \frac{s_F}{s_L} = \exp(0.057\omega_2 \chi_{H_2}^{3.3}). \tag{17}$$

This model will only apply in the low-pressure regime ($p < \Pi_c$); given the effects that EGR has on the chemistry, and the additional chemistry induced by blending with methane, the critical pressure Π_c will be a function of both the EGR and blend fraction. Understanding and predicting this value will be the focus of future work, and for cases in the high-pressure regime, an extension would have to be developed based on the form of Eq. (4).

Novelty and Significance Statement

Novel aspects of this research include rescalings to existing models for thermal diffusion to mimic multicomponent diffusion, new explanations for the enhancement of thermodiffusive instability through exhaust gas recirculation, including demonstrating the sensitivity to chemical kinetics, and an adapted model for stretch factor in hydrogen/methane blends. These findings are significant as they allow for the addition of Soret effects for minimal computational cost with good accuracy, suggests new avenues of investigation for the prediction and control of thermodiffusive instability through the addition of water and provides a simple model that could be used in lowfidelity simulations of hydrogen/methane blends.

CRediT authorship contribution statement

T.L. Howarth: Conceptualization, Data curation, Formal analysis, Investigation, Methodology, Writing – original draft, Writing – review & editing. **M.S. Day:** Conceptualization, Software, Supervision, Writing – review & editing. **H. Pitsch:** Conceptualization, Funding acquisition, Project administration, Supervision, Writing – review & editing. **A.J. Aspden:** Conceptualization, Data curation, Funding acquisition, Project administration, Resources, Supervision, Writing – review & editing.

Declaration of competing interest

The authors declare that they have no known competing financial interests or personal relationships that could have appeared to influence the work reported in this paper.

Acknowledgements

TLH and HP acknowledge funding by the European Union (ERC, HYDROGENATE, 101054894). TLH also acknowledges support provided by an EPSRC CASE Studentship with Reaction Engines Ltd. AJA is grateful for support from the Engineering and Physical Sciences Research Council (grant number EP/W034506/1). This work used the ARCHER2 UK National Supercomputing Service (https://www.archer2.ac.uk) and the Rocket HPC service at Newcastle University. This work was authored in part by the National Renewable Energy Laboratory, operated by Alliance for Sustainable Energy, LLC, for the U.S. Department of Energy (DOE) under Contract No. DE-AC36-08GO28308. This research was supported in part by the Exascale Computing Project (17-SC-20-SC), a collaborative effort of the U.S. Department of Energy Office of Science and the National Nuclear Security Administration. The views expressed in the article do not necessarily represent the views of the DOE or the U.S. Government. The U.S. Government retains and the publisher, by accepting the article for publication, acknowledges that the U.S. Government retains a nonexclusive, paid-up, irrevocable, worldwide license to publish or reproduce the published form of this work, or allow others to do so, for U.S. Government purposes.

Appendix A. Supplementary data

Supplementary material related to this article can be found online at https://doi.org/10.1016/j.proci.2024.105429.

References

[1] T.L. Howarth, A.J. Aspden, An empirical characteristic scaling model for freely–propagating lean premixed hydrogen flames, Combust. Flame 237 (2022) 111805.

[2] C. Altantzis, C. Frouzakis, A. Tomboulides, M. Matalon, K. Boulouchos, Hydrodynamic and thermodiffusive instability effects on the evolution of laminar planar lean premixed hydrogen flames, J. Fluid Mech. 700 (2012) 329–361.

[3] C.E. Frouzakis, N. Fogla, A.G. Tomboulides, C. Altantzis, M. Matalon, Numerical study of unstable hydrogen/air flames: Shape and propagation speed, Proc. Combust. Inst. 35 (1) (2015) 1087–1095.

[4] L. Berger, A. Attili, H. Pitsch, Intrinsic instabilities in premixed hydrogen flames: Parametric variation of pressure, equivalence ratio, and temperature. Part 1–dispersion relations in the linear regime, Combust. Flame 240 (2022) 111935.

[5] S. Kadowaki, H. Suzuki, H. Kobayashi, The unstable behavior of cellular premixed flames induced by intrinsic instability, Proc. Combust. Inst. 30 (1) (2005) 169–176.

[6] L. Berger, K. Kleinheinz, A. Attili, H. Pitsch, Characteristic patterns of thermodiffusively unstable premixed lean hydrogen flames, Proc. Combust. Inst. 37 (2) (2019) 1879–1886.

[7] M. Day, J. Bell, P.-T. Bremer, V. Pascucci, V. Beckner, M. Lijewski, Turbulence effects on cellular burning structures in lean premixed hydrogen flames, Combust. Flame 156 (5) (2009) 1035–1045.

[8] A.J. Aspden, M.S. Day, J.B. Bell, Turbulence–flame interactions in lean premixed hydrogen: transition to the distributed burning regime, J. Fluid Mech. 680 (2011) 287–320.

[9] L. Berger, A. Attili, H. Pitsch, Synergistic interactions of thermodiffusive instabilities and turbulence in lean hydrogen flames, Combust. Flame 244 (2022) 112254.

[10] T.L. Howarth, E.F. Hunt, A.J. Aspden, Thermodiffusively–unstable lean premixed hydrogen flames: Phenomenology, empirical modelling, and thermal leading points, Combust. Flame 253 (2023) 112811.

[11] L. Berger, A. Attili, H. Pitsch, Intrinsic instabilities in premixed hydrogen flames: parametric variation of pressure, equivalence ratio, and temperature. Part 2–Non–linear regime and flame speed enhancement, Combust. Flame 240 (2022) 111936.

[12] M. Matalon, C. Cui, J.K. Bechtold, Hydrodynamic theory of premixed flames: effects of stoichiometry, variable transport coefficients and arbitrary reaction orders, J. Fluid Mech. 487 (2003) 179–210.

[13] C.K. Law, C.J. Sung, Structure, aerodynamics, and geometry of premixed flamelets, Prog. Energy Combust. Sci. 26 (4) (2000) 459–505.

[14] J.F. Grcar, J.B. Bell, M.S. Day, The Soret effect in naturally propagating, premixed, lean, hydrogen–air flames, Proc. Combust. Inst. 32 (1) (2009) 1173–1180.

[15] F. Yang, C.K. Law, C.J. Sung, H.Q. Zhang, A mechanistic study of Soret diffusion in hydrogen–air flames, Combust. Flame 157 (1) (2010) 192–200.

[16] Z. Zhou, F.E. Hernández-Pérez, Y. Shoshin, J.A. van Oijen, L.P. de Goey, Effect of Soret diffusion on lean hydrogen/air flames at normal and elevated pressure and temperature, Combust. Theory Model. 21 (5) (2017) 879–896.

[17] J. Schlup, G. Blanquart, Validation of a mixture–averaged thermal diffusion model for premixed lean hydrogen flames, Combust. Theory Model. 22 (2) (2018) 264–290.

[18] R. Sankaran, H.G. Im, Effects of hydrogen addition on the Markstein length and flammability limit of stretched methane/air premixed flames, Combust. Sci. Technol. 178 (9) (2006) 1585–1611.

[19] F. Dinkelacker, B. Manickam, S.P.R. Muppala, Modelling and simulation of lean premixed turbulent methane/hydrogen/air flames with an effective Lewis number approach, Combust. Flame 158 (9) (2011) 1742–1749.

[20] E.C. Okafor, A. Hayakawa, Y. Nagano, T. Kitagawa, Effects of hydrogen concentration on premixed laminar flames of hydrogen–methane–air, Int. J. Hydrog. Energy 39 (5) (2014) 2409–2417.

[21] L. Esclapez, M. Day, J. Bell, A. Felden, C. Gilet, R. Grout, M. Henry de Frahan, E. Motheau, A. Nonaka, L. Owen, B. Perry, J. Rood, N. Wimer, W. Zhang, PeleLMeX: an AMR Low Mach Number Reactive Flow Simulation Code without level sub-cycling, J. Open Source Softw. 8 (90) (2023) 5450.

[22] M.S. Day, J.B. Bell, Numerical simulation of laminar reacting flows with complex chemistry, Combust. Theory Model. 4 (4) (2000) 535.

[23] A. Nonaka, M.S. Day, J.B. Bell, A conservative, thermodynamically consistent numerical approach for low Mach number combustion. Part I: Single–level integration, Combust. Theory Model. 22 (1) (2018) 156–184.

[24] D.G. Goodwin, H.K. Moffat, I. Schoegl, R.L. Speth, B.W. Weber, Cantera: An Object–oriented Software Toolkit for Chemical Kinetics, Thermodynamics, and Transport Processes, 2023, Version 3.0.0.

[25] S. Chapman, T.G. Cowling, The Mathematical Theory of Non–Uniform Gases: An Account of the Kinetic Theory of Viscosity, Thermal Conduction and Diffusion in Gases, Cambridge University Press, 1970.

[26] C.A. Hall, R.W. Pitz, Numerical simulation of premixed H2—air cellular tubular flames, Combust. Theory Model. 20 (2) (2016) 328–348.

[27] ANSYS Chemkin theory manual 17.0, 2015, Reaction Design, San Diego.

[28] J. Schlup, G. Blanquart, A reduced thermal diffusion model for H and H2, Combust. Flame 191 (2018) 1–8.

[29] A. Kazakov, M. Frenklach, Reduced Reaction Sets Based on GRI–Mech 1.2, University of California at Berkeley, Berkeley, CA, 1994, http://www.me.berkeley.edu/drm.

[30] J. Li, Z. Zhao, A. Kazakov, F.L. Dryer, An updated comprehensive kinetic model of hydrogen combustion, Int. J. Chem. Kinet. 36 (10) (2004) 566–575.

[31] M.P. Burke, M. Chaos, Y. Ju, F.L. Dryer, S.J. Klippenstein, Comprehensive H2/O2 kinetic model for high–pressure combustion, Int. J. Chem. Kinet. 44 (7) (2012) 444–474.

[32] C.K. Law, Propagation, structure, and limit phenomena of laminar flames at elevated pressure, Combust. Sci. Technol. 178 (1–3) (2006) 335–360.

[33] N. Bouvet, F. Halter, C. Chauveau, Y. Yoon, On the effective Lewis number formulations for lean hydrogen/hydrocarbon/air mixtures, Int. J. Hydrog. Energy 38 (14) (2013) 5949–5960.

[34] S. Zitouni, D. Pugh, A. Crayford, P. Bowen, J. Runyon, Lewis number effects on lean premixed combustion characteristics of multi-component fuel blends, Combust. Flame 238 (2022) 111932.

[35] J.B. Zenou, R. Vicquelin, Acceleration of premixed H2-Air-Steam flames when accounting for thermal radiation, Combust. Flame 258 (2023) 113068.